Potentiometric CO sensors using anion-conducting polymer electrolyte: Effects of the kinds of noble metal-loaded metal oxides as sensing-electrode materials on CO-sensing properties

Takeo Hyodo*, Mari Takamori, Toshiyuki Goto, Taro Ueda, and Yasuhiro Shimizu

Graduate School of Engineering, Nagasaki University

1-14 Bunkyo-machi, Nagasaki 852-8521, Japan

*Corresponding author:

Takeo Hyodo, Dr.

Graduate School of Engineering, Nagasaki University

1-14 Bunkyo-machi, Nagasaki 852-8521, Japan

Tel: +81-95-819-2644

Fax: +81-95-819-2643

E-mail: hyodo@nagasaki-u.ac.jp

Abstract

Potentiometric CO-sensing properties of electrochemical gas sensors using an anion-conducting polymer as an electrolyte and a metal oxide (MO; Bi_2O_3, CeO_2, In_2O_3, SnO_2, or V_2O_5) loaded with or without 2.0 wt% noble metal (N; Ag, Au, Ir, Ru, Rh, Pd, or Pt) as an electrode material (EC(N/MO) or (EC(MO) sensor; N/MO: N-loaded MO) were investigated in wet synthetic air (57%RH) at 30ºC. Among all the EC(MO) sensors, the EC(CeO_2) sensor showed the largest CO response and excellent CO selectivity against H_2 and the EC(Bi_2O_3) sensor showed relatively large CO and H_2 responses (no CO selectivity against H_2). Other EC(MO) sensors hardly showed both CO and H_2 responses. However, the Au loading just onto In_2O_3 and SnO_2 was effective in improving the magnitude of CO and H_2 responses of the EC(In_2O_3) and EC(SnO_2) sensors, respectively, which resulted in relatively poor CO selectivity against H_2. On the other hand, the Pt loading only onto SnO_2 extremely enhanced only the magnitude of CO response of the EC(SnO_2) sensor, and thus the EC(Pt/SnO_2) sensor showed the most excellent CO selectivity against H_2, among all the sensors in this study. The heat treatment of N/MO powders in H_2 at 250°C reduced only the H_2 response of the EC(Au/SnO_2) sensor, leading to an improvement of the CO selectivity of only the EC(Au/SnO_2) sensor against H_2. On the other hand, the heat treatment drastically enhanced both CO and H_2 responses of the EC(Pt/SnO_2) sensor, resulting in a decrease in its CO selectivity against H_2. The CO and H_2 responses of other EC(N/SnO_2) sensors before and after the heat treatment in H_2 at 250°C were also examined, and the effectiveness of the noble metal loading and the heat treatment on the CO-sensing properties was discussed in this study. In addition, gas-sensing mechanism was also proposed on the basis of chemical surface states of representative N/MO.

***Keywords*:** Potentiometric gas sensor; Anion-conducting polymer; Carbon monoxide; Metal oxide; Noble metal

1. Introduction

Carbon monoxide (CO) is extremely harmful to human health, because CO can quickly combine with hemoglobin in human blood and then seriously interfere with the transport of oxygen to tissues in human body [1]. However, we cannot detect CO, which is odorless and colorless, by ourselves, and thus highly sensitive and selective CO sensors are quite essential in detecting even a low concentration of CO quickly and accurately, and then in preventing inhalation of CO into lung through the respiratory system. Among various types of CO sensors [2–6], electrochemical gas sensors using cation-conducting polymer (such as Nafion®) as an electrolyte material, which can be operated at RT, have also been attractive as a high performance CO sensor [7–13], and some types of electrochemical CO sensors are presently commercialized all over the world [14]. On the other hand, anion-conducting polymers (ACP) with large OH^- conductivity and improved long-term stability [15–17] are also quite attractive as an electrolyte material alternative to cation-conducting polymers, because most of metal oxides are relatively stable in alkaline media. We have already demonstrated that potentiometric gas sensors employing the ACP electrolyte and Pd- or Pt-loaded carbon-black electrodes showed relatively large responses to H_2 [18], CO [19], and CO_2 [20], respectively, but gas selectivity of these sensors was really poor. Therefore, we have recently investigated CO-sensing properties of the ACP-based sensors using a metal oxide (Co_3O_4, In_2O_3, SnO_2, or ZnO) loaded with Au nanoparticles as a CO-sensing electrode material, and reported that the use of Au-loaded In_2O_3 or SnO_2 electrodes drastically enhanced the magnitude of CO response as well as CO selectivity against H_2 after heat treatment of the Au-loaded In_2O_3 or SnO_2 powder under a reducing atmosphere at an elevated temperature (250°C) [21, 22]. These results obviously show that such metal-oxide-based materials have substantial advantage in the CO-sensing properties (especially, the CO selectivity against H_2), as a CO-sensing electrode substrate of potentiometric gas sensors, in comparison with carbon-black-based materials.

Therefore, we have attempted to find promising metal oxides loaded with noble metal as a highly sensitive and selective CO-sensing electrode material of potentiometric gas sensors in this study. First, we have discussed effects of the kind of metal oxide (Bi_2O_3, CeO_2, In_2O_3, SnO_2, or V_2O_5) as a base material of the sensing electrode on the CO-sensing properties of the ACP-based sensors. In addition, the impacts of the kind of noble metal (Ag, Au, Ir, Ru, Rh, Pd, or Pt) loaded onto the SnO_2 powder and the heat-treatment conditions on their CO-sensing properties have been also investigated.

2. Experimental

2.1. Preparation of metal-oxide (MO) powders

Five kinds of MO powders (Bi_2O_3, CeO_2, In_2O_3, SnO_2, V_2O_5) were prepared according to the following procedure.

[Bi_2O_3] The pH of a 0.20 M $Bi(NO_3)_3$ aqueous solution was adjusted to 11 by the addition of a NaOH aqueous solution. The obtained precipitate was centrifuged and washed with pure water repeatedly, and then it was dried at 100°C. The resultant dried powder was calcined at 500°C for 3 h in air, to obtain a Bi_2O_3 powder.

[CeO_2] A 0.02 mol $Ce(NO_3)_3 \cdot 6H_2O$ was dissolved into ethanol (30 cm^3), and then 0.16 mol triethanolamine and 300 cm^3 pure water were added into the solution. The obtained precipitate was centrifuged and washed with pure water and methanol sometimes. A CeO_2 powder was prepared by the calcination of the resultant powder at 700°C for 2 h in air.

[In_2O_3 and SnO_2] The pH of 0.35 M $In(NO_3)_3$ or 0.17 M $SnCl_4$ aqueous solution was adjusted to 3.5 and 2.0, respectively, by the addition of a NH_3 aqueous solution. The obtained precipitate was centrifuged and washed with pure water repeatedly, and then dried at 100°C. Then, In_2O_3 or SnO_2 powder was prepared by the calcination of the resultant powder at 500°C for 3 h in air.

[V_2O_5] After an appropriate amount of NH_4VO_3 and oxalic acid was added into pure water, the

solution was evaporated to dryness. The obtained precipitate was centrifuged and washed with pure water repeatedly, and then dried at 100°C. After crushing the resultant solid by using an agate mortar, a V_2O_5 powder were prepared by the calcination of the powder at 500°C for 3 h in air.

2.2. Preparation of MO powders loaded with 2 wt% noble metal (N)

Loading of Au nanoparticles on the MO powders was only performed by general precipitation-deposition technique [23]. After the pH value of a 1 mM $HAuCl_4$ aqueous solution at 70°C was adjusted to 4 by addition of a NH_3 aqueous solution, the MO powder (2.0 g) was added to the solution (197 cm^3). The pH value of the solution was adjusted to 7.0 by further addition of an NH_3 aqueous solution and the solution was stirred at 70°C for 1 h, to deposit Au-based precipitates ($Au(OH)_3$) on the surface of the MO powder, and then it was centrifuged and repeatedly washed with pure water. The obtained powder was dried at 100°C and then heat-treated at 400°C for 1 h in air or at 250°C for 1 h in H_2, to obtain 2 wt% Au-loaded MO powders. Their powders heat-treated in air or H_2 was referred to as Au/MO or Au/MO-h, respectively. Other N-loaded MO powders were prepared by general impregnation technique. After an appropriate amount of each MO powder was added to a 1 mM $Ag(NO_3)$, $IrCl_3$, $RuCl_3$, $RhCl_4$, $Pd(NO_3)_2$, or $PtCl_4$ aqueous solution, the obtained solution containing a MO powder was ultrasonicated at RT for 10 min and then it was evaporated to dryness. Then, the resultant solid was heat-treated in air at 500°C for 1 h or in H_2 at 250°C for 1 h. The obtained 2.0 wt% N-loaded MO powders heat-treated in air or H_2 were denoted as N/MO or N/MO-h, respectively.

2.3. Characterization of all powders

Crystal phases of all powders prepared were characterized by X-ray diffraction analysis (XRD; Rigaku Corp., RINT2200) using Cu Kα radiation (40 kV, 36 mA), and their crystallite

sizes (CS) were calculated by utilizing the Scherrer equation (shaper factor: 0.9). Pore size distributions and specific surface areas (SSA) of all the powders were measured by general Barrett-Joyner-Halenda (BJH) and Brunauer-Emmett-Teller (BET) methods using N_2 adsorption-desorption isotherms (Micromeritics Inst. Corp., TriStar 3000), respectively. Chemical states of elements on the surface of representative N/MO powders (N: Au and Pt, MO: Bi_2O_3, In_2O_3, and SnO_2) were characterized by X-ray photoelectron spectroscopy using Al Kα radiation (XPS, Kratos, ACIS-TLATRA DLD), and the binding energy was calibrated using the C 1s level (285.0 eV) from usual contamination.

2.4. Fabrication of potentiometric gas sensors and measurement of their CO- and H_2-sensing properties

A schematic drawing of a sensor element, or an electrochemical cell, is shown in Fig. 1(a). The MO or N/MO powder was mixed with an ACP solution (AS-4, Tokuyama Corp.), which is an *iso*-propanol containing a 5 wt% hydrocarbon-type ionic polymer with quaternary ammonium salts (MO or N/MO powder : ACP = 95 : 5 in weight) [15, 16]. The paste obtained was applied on the surface of both sides of an ACP membrane (A201, Tokuyama Corp., a polyolefin polymer film which consists of hydrocarbon main chain and quaternary ammonium salts, thickness: ca. 30 μm [15, 16]) as sensing and counter electrodes by blade coating, and then it was dried at ca. 50°C for 30 min. The sensor element fabricated with MO or N/MO powder was denoted as EC(MO) or EC(N/MO), respectively (EC stands for electrochemical cell). In addition, the sensor element was also fabricated by utilizing commercial Au paste (TR-1403, Tanaka Kikinzoku Kogyo K.K.) or Pt paste (TR-7907, Tanaka Kikinzoku Kogyo K.K.) as a blade-coating material, and it was denoted as EC(Au) or EC(Pt), respectively.

A schematic drawing of a gas-sensing measurement system with two electrode compartments is shown in Fig. 1(b). The fabricated sensor element was sandwiched with Au

meshes (Nilaco, 100 mesh) as a current collector and was set up in a gas-sensing measurement system with two electrode compartments. Electromotive force (E) of all sensors to CO or H_2 (10–3000 ppm) balanced with wet synthetic air (O_2: 20%, N_2: 80%, relative humidity: 57%RH at 30°C), which was flowed over the sensing electrode, was measured at 30°C by using a digital electrometer (ADCMT, 8240), while the wet synthetic air was flowed over the counter electrode. The magnitude of response was defined as a change in E value induced by a sample gas (ΔE_{SG}, SG (sample gas): CO or H_2). CO selectivity against H_2 was defined as a ratio of CO response to H_2 response ($\Delta E_{CO}/\Delta E_{H_2}$).

3. Results and Discussions

3.1. CO-sensing properties of EC(MO) sensors and effects of Au or Pt loading onto MO

Figure S1 shows XRD spectra of all MO powders, together with their crystallite sizes (CS) which were calculated from (120), (111), (222), (110), and (110) diffraction peaks of Bi_2O_3, CeO_2, In_2O_3, SnO_2, and V_2O_5 powders, respectively. In addition, Figure S2 shows N_2 adsorption-desorption isotherms and pore-size distributions of their powders, together with their specific surface areas (SSA). The XRD spectrum of each MO powder, which was prepared with a $Bi(NO_3)_3$, $Ce(NO_3)_3$, $In(NO_3)_3$, $SnCl_4$, or NH_4VO_3 aqueous solution was attributed to a single phase of Bi_2O_3 (JCPDS No. 71-2274), CeO_2 (JCPDS No. 65-5923), In_2O_3 (JCPDS No. 89-4595), SnO_2 (JCPDS No. 41-1445), or V_2O_5 (JCPDS No. 41-1426), respectively. The CS value of the prepared Bi_2O_3, CeO_2, In_2O_3, SnO_2, or V_2O_5 powder was ca. 54.5, 25.5, 19.8, 8.9, or 71.6 nm, respectively. On the other hand, the SSA value of the prepared Bi_2O_3, CeO_2, In_2O_3, SnO_2, or V_2O_5 powder was ca. 0.903, 19.3, 37.6, 41.4, 2.49 $m^2\ g^{-1}$, respectively. The N_2 adsorption-desorption isotherms of the CeO_2, In_2O_3, and SnO_2 powders, which had relatively large SSAs, belong to "Type IV" according to the BET classification [24], because of an abrupt and quite small increase in volume of adsorbed N_2 at low P/P_0 range (≤ 0.2), small positive

slope at a medium P/P_0 range and the abrupt and large increase in volume of adsorbed N_2 and hysteresis at a high P/P_0 range. The hysteresis behavior is associated with capillary condensation and evaporation of N_2 in and from their well-developed ink-bottle mesopores, respectively, and thus these powders showed relatively large SSAs. Besides, the size of mesopores of the In_2O_3 powder was the largest, followed by those of the SnO_2 and CeO_2 powders. On the other hand, the N_2 adsorption-desorption isotherms of the Bi_2O_3 and V_2O_5 powders, which had quite small SSAs, basically belong to "Type II" [24], and thus the number of pore volumes of their mesopores were extremely small. However, the dependence of CS on the kinds of MO was not necessarily correspondent on that of SSA. Therefore, the geometric surface areas (GSAs) of the MO powders were calculated from CSs obtained from their XRD spectra (Fig. S1) and their densities (8.90, 7.22, 7.18, 6.95, and 3.36 g cm^{-3} for Bi_2O_3, CeO_2, In_2O_3, SnO_2, and V_2O_5, respectively [25]), assuming that the morphology of their crystallites is spherical, and the relationship between two kinds of surface areas (SSA and GSA) and CS of all the MO powders is shown in Fig. S3. The ratios of GSA to SSA (GSA/SSA values) of the CeO_2, In_2O_3, and SnO_2 powders with relatively large SSAs were quite small, which indicated that many voids among their meso-sized crystallites were the origins of well-developed ink-bottle mesopores. Especially, the smallest GSA/SSA value of the In_2O_3 powder (ca. 1.1) showed that most all of the crystallites did not strongly agglomerate each other and thus gaseous species was easily able to access to the most surface and boundary of the crystallites. On the other hand, the Bi_2O_3 and V_2O_5 powders showed quite large GSA/SSA values as well as small SSAs. This means that most of their large crystallites agglomerated each other and there were little voids forming mesopores.

Figures 2 and 3 show response transients of all EC(MO), EC(Au/MO), and EC(Pt/MO) sensors to 500 ppm CO and 500 ppm H_2, respectively, at 30°C in wet synthetic air (57%RH), and Table S1 summaries the magnitude of their CO and H_2 responses and CO selectivity against

H_2. Among all the EC(MO) sensors, the EC(Bi_2O_3) sensor showed relatively large responses to both CO and H_2. The magnitude of CO response (ΔE_{CO}: ca. 30 mV) was quite similar to that of H_2 (ΔE_{H_2}: ca. 30 mV, the largest among all the EC(MO) sensors), which indicated that the EC(Bi_2O_3) had no CO selectivity against H_2 ($\Delta E_{CO}/\Delta E_{H_2}$: ca. 1.0). Considering the large CS, small SSA, and undeveloped pore-size distribution (small pore volume) of the Bi_2O_3 powder, the responses to both CO and H_2 of EC(Bi_2O_3) sensor may arise only from the relatively large electrocatalytic activity of CO and H_2 oxidation over Bi_2O_3 even at lower temperatures. However, the loading of Au or Pt onto Bi_2O_3 slightly increased the electromotive force (E) of the EC(Bi_2O_3) sensor in synthetic air, only slightly increased or decreased the magnitude of both CO or H_2 responses, respectively, and hardly improved the response and recovery speeds as well as the CO selectivity against H_2. Namely, the loading of Au or Pt onto Bi_2O_3 was less effective in improving the CO-sensing properties of the EC(Bi_2O_3) sensor. The EC(CeO_2) sensor showed the largest CO response (ΔE_{CO}: ca. 33 mV) among all the EC(MO) sensors, probably because of the relatively large electrocatalytic activity of CO oxidation over CeO_2 [26]. However, the response and recovery speeds of the EC(CeO_2) sensor were much slower than those of the EC(Bi_2O_3) sensor. The magnitude of H_2 response was quite small (ΔE_{H_2}: ca. 3 mV), and thus the sensor showed the largest CO selectivity against H_2 ($\Delta E_{CO}/\Delta E_{H_2}$: ca. 11) among all the EC(MO) sensors. The Au loading onto the CeO_2 slightly improved the magnitude of CO response (ΔE_{CO}: ca. 36 mV) and moderately enhanced the magnitude of H_2 response (ΔE_{H_2}: ca. 17 mV), and thus decreased the CO selectivity against H_2 ($\Delta E_{CO}/\Delta E_{H_2}$: ca. 1.9). However, the Pt loading was ineffective in improving the sensing behavior to CO and H_2. The EC(V_2O_5) sensor showed no CO and H_2 responses and the loading of Au or Pt onto the V_2O_5 did not improve the sensing behavior to CO and H_2 at all. In addition, the electromotive force of some EC(MO) and EC(N/MO) sensors in base gas (especially, MO: CeO_2 and V_2O_5) often shifted irregularly and unsteadily, due to the quite large resistance of CeO_2 and V_2O_5 at 30°C.

On the other hand, both the EC(In_2O_3) and EC(SnO_2) sensors hardly showed CO and H_2 responses, but the loading of Au or Pt onto both In_2O_3 and SnO_2 drastically improved the CO and/or H_2 responses in some cases. The Au loading onto In_2O_3 and SnO_2 largely improved the CO responses of the EC(In_2O_3) and EC(SnO_2) sensors (ΔE_{CO}: ca. 90 mV for the EC(Au/In_2O_3) sensor, ca. 100 mV for the EC(Au/SnO_2) sensor), respectively, with the slight overshooting behavior [17, 18]. However, the CO selectivity of the EC(Au/In_2O_3) and EC(Au/SnO_2) sensors against H_2 ($\Delta E_{CO}/\Delta E_{H_2}$: ca. 2.4 and ca. 2.3, respectively) was much smaller than we had expected, because the magnitude of H_2 response of the EC(Au/In_2O_3) and EC(Au/SnO_2) sensors was also moderately large (ΔE_{H_2}: ca. 37 mV and ca. 44 mV, respectively). Meanwhile, the Pt loading onto In_2O_3 was hardly effective in improving the CO-sensing properties. However, the Pt loading onto SnO_2 drastically enhanced the magnitude of CO response (ΔE_{CO}: ca. 120 mV), and the CO selectivity of the EC(Pt/SnO_2) sensor against H_2 was quite large ($\Delta E_{CO}/\Delta E_{H_2}$: ca. 10), since the magnitude of H_2 response was quite small (ΔE_{H_2}: ca. 12 mV). It is interesting to note that the response and recovery speeds of the EC(Pt/SnO_2) sensor to CO was slower than those of the EC(Au/SnO_2) sensor.

3.2. Sensing mechanism of EC(N/MO) sensors to CO and H_2

XPS analyses of representative N/MO powders (N: Au or Pt, MO: Bi_2O_3, In_2O_3, SnO_2) were conducted in order to clarify the effects of the loading of Au or Pt on the CO-sensing properties of the EC(N/MO) sensors. Figures 4, 5, and 6 show their XPS spectra of N (Au and Pt) $4f_{7/2}$ and $4f_{5/2}$, M (Bi $4f_{7/2}$, In $4f_{7/2}$, and Sn $3d_{5/2}$), and O 1s, respectively. Most of Au atoms of these Au/MO powders existed as a metal. However, the binding energy of Au of Au/Bi_2O_3 was the largest among them, and the binding energy of Au of Au/In_2O_3 was slightly smaller than that of Au/SnO_2. This indicates that the electron density of Au particles loaded on the surface of Au/In_2O_3 was the largest, followed by those of Au/SnO_2 and Au/Bi_2O_3. On the other hand, most

of Pt atoms of these Pt/MO powders were basically oxidized, and the oxidation state was largely dependent on the kinds of the oxides. Pt of Pt/SnO_2 was most oxidized among them, and the Pt/SnO_2 had a large amount of Pt^{4+} and a medium amount of Pt^{2+}, together with a quite small amount of Pt metal. Hübner et al. [27] and Murata et al. [28] have investigated the composition and chemical state of thick Pt/SnO_2 films which were fabricated by screen printing and thin Pt-SnO_2 composite films which were fabricated with magnetron sputtering using a Pt/SnO_2 target, respectively, and they have suggested that the relatively large amount of Pt was doped into the SnO_2 lattice and the Pt^{n+} species (the doping amount: ≤ ca. 10 at%, according to the results by Murata et al. [28]) were located at the Sn position in the rutile structure. Considering the analyses of the Pt-SnO_2 composite films with X-ray adsorption fine structure (XAFS) spectroscopy and XPS by Murata et al., the preparation technique of the Pt/SnO_2 powder in this study, and the radii of 6-coordinate ions (Pt^{4+}: 0.625 Å, Pt^{2+}: 0.80 Å, Sn^{4+}: 0.83 Å [29]), it was expected that most of Pt^{4+} and Pt^{2+} were doped into the Sn^{4+} sites in the lattice at the SnO_2 surface and a slight number of Pt-based nanoparticles, which had oxidized surface such as PtO and/or PtO_2, were loaded onto the SnO_2 surface. On the other hand, the main peaks of both Pt/Bi_2O_3 and Pt/In_2O_3 originated from Pt^{2+}, and the ratio of the amount of Pt^{2+} to the amount of Pt^{4+} of Pt/Bi_2O_3 seemed to be larger than that of Pt/In_2O_3. Since the radii of 6-coordinate Bi^{3+} and In^{3+} species (Bi^{3+}: 1.03 Å, In^{3+}: 0.800 Å [29]) are larger than that of 6-coordinate Pt^{4+} and Pt^{2+} species, both the Pt^{4+} and Pt^{2+} species can be doped also into the Bi^{3+} and In^{3+} sites in the lattice at the Bi_2O_3 and In_2O_3 surfaces, respectively. As the small peak of Pt metal was also clearly confirmed in the XPS spectra of both Pt/In_2O_3 and Pt/Bi_2O_3, a small number of Pt metal nanoparticles were loaded on both the surfaces and the surface of the Pt metal nanoparticles may be also oxidized to be PtO and PtO_2. Besides, the electron density of all the Pt species on the surface of Pt/SnO_2 was the largest, followed by those of Pt/In_2O_3 and Pt/Bi_2O_3, according to their binding energies.

On the other hand, the binding energy of Bi 4f of N/Bi_2O_3 was independent of the kind of N and the binding energy of Sn 3d of Pt/SnO_2 was slightly larger than that of Au/SnO_2, while the binding energy of In 4f of Pt/In_2O_3 was much larger than that of Au/In_2O_3 (namely, the electron density of In^{3+}: Au/In_2O_3 > Pt/In_2O_3), as shown in Fig. 5. In the O 1s spectra, a large peak derived from lattice oxygen species and a small peak derived from adsorbed oxygen species and/or hydroxyl group were confirmed as shown in Fig. 6. In addition, their binding energies (N/Bi_2O_3 < N/In_2O_3 < N/SnO_2) are also dependent on the kinds of oxides (namely, the electron density: N/Bi_2O_3 > N/In_2O_3 > N/SnO_2). The kind of noble metal (N, Au or Pt) had no effect on the spectra of N/Bi_2O_3 and N/SnO_2, while the binding energy of Pt/In_2O_3 was larger than that of Au/In_2O_3.

On the basis of sensing properties to CO and H_2 and surface analyses by XPS, the gas-sensing mechanism was discussed as follows. Our previous studies have already demonstrated that the mixed potential resulting from electrochemical oxygen reduction (eq. (1)) and electrochemical CO oxidation (eq. (2)) generally determines the sensing-electrode potential of the potentiometric gas sensors in CO balanced with wet synthetic air [21, 22].

$$(1/2)O_2 + H_2O + 2e^- \rightarrow 2OH^- \quad (1)$$

$$CO + 2OH^- \rightarrow CO_2 + H_2O + 2e^- \quad (2)$$

Actually, the relationship between the magnitude of CO response and the concentration in synthetic air was quite linear [21, 22]. The Au loading largely improved both the CO responses of only the EC(In_2O_3) and EC(SnO_2) sensors among all the EC(MO) sensors and the magnitude of these CO responses was much larger than that of these H_2 responses, as shown in Figs. 2 and 3. In addition, we have already reported that the Au species was uniformly loaded as nano-sized particles on the surface of In_2O_3 and SnO_2 powders [21, 22], and the XPS analyses (Fig. 4) showed that the electron density of Au nanoparticles loaded on the Au/In_2O_3 and Au/SnO_2 surfaces was larger than that of Au nanoparticles loaded on the Au/Bi_2O_3 surface. CO molecules

are well known to be adsorbed on the step, edge, and corner sites of Au nanoparticles as well as Au/MO interfaces, while O_2 molecules are activated at the Au/MO interfaces by the reaction with water molecules. Thereafter, these CO adsorbates reacted with the activated oxygen species at the Au/MO interfaces, to form CO_2 [30–32]. Based on this mechanism of catalytic CO oxidation under gaseous atmosphere, CO molecules should be adsorbed on Au nanoparticles on the surface of In_2O_3 and SnO_2, also in this study. In addition, it was also confirmed that the binding energies of In 4f and O 1s of Au/In_2O_3 were smaller than those of Pt/In_2O_3 (namely, electron density of In^{3+} and O^{2-} of Au/In_2O_3 was larger than that of Pt/In_2O_3.). These results indicate that the loading of Au nanoparticles partially and slightly reduced the surface of In_2O_3 and SnO_2 and/or formed oxygen vacancies at the surface in some cases, especially around the Au/MO interfaces. Therefore, the Au/MO interfaces worked as electrochemically active redox sites, where the oxidation of the large number of CO adsorbates on the surface of Au and the Au/MO interfaces and the reduction of oxygen adsorbates simultaneously proceeded.

H_2 molecules are electrochemically oxidized in alkaline media, as shown below.

$$H_2 + 2OH^- \rightarrow 2H_2O + 2e^- \quad (3)$$

It was already reported that the rate of dissociative adsorption of H_2 molecules is quite slow on the surface of Au nanoparticles [33] and the dissociation mainly proceeds at Au/MO interfaces, together with adsorption and activation of oxygen molecules at the same sites [34]. Actually, the Au loading improved the H_2 responses of the EC(In_2O_3) and EC(SnO_2) sensors. Therefore, the Au/MO interfaces must work as electrochemically oxidation sites for adsorbed hydrogen species, also in this study. However, the magnitude of these H_2 responses was smaller than that of these CO responses, as shown in Figs. 2 and 3, probably because the number of hydrogen adsorbates at the Au/MO interfaces was much smaller than that of CO adsorbates on the Au surface as well as at the Au/MO interfaces.

On the other hand, the EC(Bi_2O_3) sensor showed the largest CO and H_2 responses among all the EC(MO) sensors. The Bi_2O_3, which has some oxygen vacancies in the lattice [35], has been applied as a component of various oxidation catalysts to organic molecules [36], CO [37], and H_2S [38]. We also have reported that the Bi_2O_3 addition into Pt electrode largely enhanced the CO-sensing properties of NASICON-based solid electrolyte gas sensors at RT [39]. These properties support that the electrochemical oxidation activity of both CO and H_2 are relatively active over the Bi_2O_3 surface (e.g., via oxygen vacancy [40]). However, the Au loading was ineffective in improving the CO and H_2 responses of the EC(Bi_2O_3) sensor. Fig. 4(a)(i) showed that electron density of Au nanoparticles on the Bi_2O_3 surface was smaller than that on In_2O_3 and SnO_2. This result shows that the chemical and electrical interaction is really small between Au and Bi_2O_3. Therefore, the number of CO adsorbates and dissociatively adsorbed hydrogen species as well as the number of activated oxygen adsorbates was quite small at Au/Bi_2O_3 interfaces, and the CO molecules adsorbed on the Au surface were not also effectively oxidized at the Au/Bi_2O_3 interfaces. The inactive Au/Bi_2O_3 interfaces are probably the most important key in eliminating the effect of the Au loading on the CO and H_2 responses of the EC(Bi_2O_3) sensor.

The Pt loading onto SnO_2 drastically improved the EC(SnO_2) sensor as shown in Fig. 3, while Fig. 4(b) showed that most of Pt was oxidized at the Pt/SnO_2 surface (main and sub chemical states: Pt^{4+} and Pt^{2+}, respectively) and these oxidized Pt species were expected to be doped into the Sn^{4+} sites in the lattice at the SnO_2 surface [27, 28]. On the other hand, the Pt loading onto Bi_2O_3 and In_2O_3 was ineffective in improving the EC(Bi_2O_3) and EC(In_2O_3) sensors, respectively, as shown in Figs. 2 and 3, while Fig. 4(b) showed that most of Pt existed mainly as Pt^{2+} species at both the Pt/Bi_2O_3 and Pt/In_2O_3 surfaces and they were also expected to be doped into the Sn^{4+} sites in the lattice at the SnO_2 surface. In addition, the fact that electron density of all the Pt species of Pt/SnO_2 was larger than those of Pt/Bi_2O_3 and Pt/In_2O_3 (see Fig.

4(b)) indicates that Pt/SnO_2 has the relatively large number of oxygen vacancies near Pt species in the surface lattice. Moreover, CO molecules can be directly adsorbed on the active sites, while H_2 molecules should be dissociatively adsorbed on the active sites. Considering these results and discussion, CO molecules were adsorbed just on the top of Pt^{4+} and/or via oxygen vacancies next to Pt^{4+} at the surface lattice of SnO_2, and then the CO adsorbates electrochemically reacted with adjacent OH^- adsorbates, to form CO_2. O_2 molecules also were adsorbed at the same electrochemically active sites, and then they were reduced, to form OH^-. However, H_2 molecules, which need to be dissociatively adsorbed on the active sites, are difficult to be adsorbed just on the individually (singly) dispersed Pt^{4+} sites at the surface lattice. Therefore, the EC(Pt/SnO_2) sensor showed only the quite small H_2 response.

3.3. Sensing properties of EC(N) sensors (N: Au or Pt) to CO and H_2

In order to remove the effect of the base oxide materials (MO) on the sensing properties to both CO and H_2, response transients of EC(Au) and EC(Pt) sensors to 500 ppm CO and H_2 were investigated at 30°C in wet synthetic air (57%RH), as shown in Fig. 7. The magnitude of their CO and H_2 responses and CO selectivity against H_2 were summarized in Table S2. The magnitude of CO and H_2 responses of the EC(Au) sensor (ΔE_{CO}: ca. 38 mV, ΔE_{H_2}: ca. 30 mV) was larger than that of the EC(Pt) sensor (ΔE_{CO}: ca. 7.2 mV, ΔE_{H_2}: ca. 8.8 mV), and both the sensors showed poor CO selectivity against H_2 ($\Delta E_{CO}/\Delta E_{H_2}$: ca. 1.3 for the EC(Au) sensor and ca. 0.82 for the EC(Pt) sensor), which was much smaller than those of the EC(Pt/SnO_2) sensor as well as the EC(Au/SnO_2) sensor. For both the EC(Au) and EC(Pt) sensors, the electrochemical oxidation of CO (eq. (1)) and H_2 (eq. (3)) and the electrochemical reduction of O_2 (eq. (2)) at the Au and Pt sensing electrodes are expected to proceed at triple-phase boundaries consisting of gas, liquid (ACP membrane), and solid (Au and Pt). In addition, it is well known that the exchange current density of oxygen reduction at a Au electrode is much

smaller than that at a Pt electrode [41]. Therefore, the larger responses of the EC(Au) sensor to CO and H_2 than those of the EC(Pt) sensor and the quite poor CO selectivity of both the sensors against H_2 are because the electrochemical oxidation rate of CO at such triple-phase boundaries was relatively comparable to that of H_2 and the electrochemical reduction rate of O_2 at triple-phase boundaries of the Au electrode is generally much smaller than that of the Pt electrode. On the other hand, both the CO responses of the EC(Au/MO) sensor (MO: In_2O_3 or SnO_2) and the EC(Pt/SnO_2) sensor were much larger than those of the EC(Au) and EC(Pt) sensors, whereas the H_2 responses of the EC(Au/MO) sensor (MO: In_2O_3 or SnO_2) and the EC(Pt/SnO_2) sensor were comparable to those of the EC(Au) and EC(Pt) sensors, respectively. Therefore, these results indicate that the oxide surface of the Au/MO (MO: In_2O_3 or SnO_2) and Pt/SnO_2 sensing electrodes serves a quite important function as a part of the reaction sites especially for the electrochemical CO oxidation, and thus the combination of the oxide surface with Au or Pt nanoparticles at these sensing electrodes enhanced only the magnitude of CO responses for the EC(Au/MO) sensor (MO: In_2O_3 or SnO_2) and the EC(Pt/SnO_2) sensors.

3.4. Sensing properties of EC(N/SnO_2) sensors to CO and H_2

Effects of the kinds of noble metal (N) loaded onto SnO_2 on the sensing properties of EC(N/SnO_2) sensors to CO and H_2 were also investigated in this study. Figure 8 shows response transients of all the EC(N/SnO_2) sensors to 500 ppm CO and H_2 at 30°C in wet synthetic air (57%RH). The magnitude of their CO and H_2 responses and CO selectivity against H_2 were summarized in Table S3. The EC(Au/SnO_2) and EC(Pt/SnO_2) sensors showed large CO responses with relatively small H_2 responses, as shown in Section 3.2. On the other hand, the other EC(N/SnO_2) sensors (N: Ag, Ir, Rh, and Ru), which did not involve the EC(Pd/SnO_2) sensor, showed little CO and H_2 responses. The EC(Pd/SnO_2) sensor unstably showed the large CO response (ΔE_{CO}: ca. 56 mV) with too large overshooting behavior. In addition, the

electromotive force (E) of the sensor in wet synthetic air (base gas) gradually tended to shift positively after exposure to CO, and the E value attained to ca. 111 mV in wet synthetic air, before the H_2-sensing property of the sensor was measured. The magnitude of H_2 response of this sensor toward the E value (ΔE_{H_2}: ca. 95 mV) was larger than that of the CO response, and thus the CO selectivity against H_2 was quite small ($\Delta E_{CO}/\Delta E_{H_2}$: ca. 0.59). These results indicate that the exposure to reducing gases such as CO and H_2 in wet synthetic air changed the chemical states of Pd species and/or SnO_2. Actually, the color of the Pd/SnO_2 sensing electrode largely changed from gray to black after the measurement, even though the color of the counter electrode only after exposure to a base gas (wet synthetic air) didn't change. Therefore, XPS analyses of the sensing electrodes of the EC(Pd/SnO_2) sensor were performed before and after exposure to 3000 ppm CO and H_2 balanced with wet synthetic air for 2 h, as shown in Fig. 9 and Fig. S4. XPS spectra of Sn $3d_{5/2}$ and O 1s of all the sensing electrodes were hardly influenced even by exposure to the highly concentrated CO and H_2 atmospheres balanced with wet synthetic air (Fig. S4). However, the binding energies of both the XPS spectra of both the components of all the electrodes were smaller than those of the Au/SnO_2 and Pt/SnO_2 powders (see Figs. 5 and 6), because of the large number of oxygen vacancies as well as the large electron density of Sn and O species by the loading of Pd species on the SnO_2 surface. On the other hand, XPS spectra of Pd 3d of the sensing electrodes was sensitive to the gaseous atmosphere. Namely, most of the Pd component on the SnO_2 surface was PdO before exposure to CO or H_2, but the exposure to CO or H_2 surprisingly oxidized a part of the PdO species to form PdO_2. The electrochemical oxidation of CO or H_2 and electrochemical reduction of O_2, which simultaneously proceed at the sensing electrode under the gaseous atmospheres, must have induced the oxidation from PdO to PdO_2, but we don't have sufficient information to understand the mechanism at present. However, the change in the chemical states of the Pd species can explain a rise in the electromotive force (E) of the EC(Pd/SnO_2) sensor with exposure to CO

and H_2 balanced with wet synthetic air, because the standard redox potentials of Pd/PdO and PdO/PdO_2 are +0.896 and +1.283 V (vs. SHE), respectively. As such increase in the electromotive force was not confirmed when carbon black was utilized as a base electrode material for the Pd loading in spite of SnO_2 [19, 20], the chemical properties of the SnO_2 surface have a large influence on the stability of PdO species in CO or H_2 balanced with wet synthetic air.

Our previous studies have demonstrated that heat treatment of the Au/SnO_2 powder under H_2 atmosphere at 250°C reduced the magnitude of H_2 response of the EC(Au/SnO_2) sensor, while maintaining the large CO response, and thus it drastically improved the CO selectivity against H_2 [22]. Therefore, all the N/SnO_2 powders prepared in this study were also heat-treated at the same reducing condition (in H_2 at 250°C for 2 h), the effects of the heat treatment of the N/SnO_2 powders on the CO-sensing properties. Figure 10 shows response transients of all the EC(N/SnO_2-h) sensors to 500 ppm CO and H_2 at 30°C in wet synthetic air (57%RH), and Table S3 summarizes the magnitude of their CO and H_2 responses and CO selectivity against H_2. The heat treatment of the Au/SnO_2 powder in H_2 drastically decreased the H_2 response (ΔE_{H_2}: ca. 3 mV), with maintaining the magnitude of CO response (ΔE_{CO}: ca. 100 mV) and thus the EC(Au/SnO_2-h) sensor showed excellent CO selectivity against H_2 ($\Delta E_{CO}/\Delta E_{H_2}$: ca. 33), also as shown in our previous report [22]. The only decrease in the H_2 response may arise from a decrease in the number of dissociatively adsorbed hydrogen species at Au/SnO_2 interfaces. On the other hand, the CO and H_2 responses of the EC(Pt/SnO_2-h) sensor (ΔE_{CO}: ca. 221 mV, ΔE_{H_2}: ca. 118 mV) were much larger than those of the EC(Pt/SnO_2) sensor (ΔE_{CO}: ca. 120 mV, ΔE_{H_2}: ca. 12 mV, see Fig. 3), but thus the CO selectivity the EC(Pt/SnO_2-h) sensor against H_2 was quite small ($\Delta E_{CO}/\Delta E_{H_2}$: ca. 1.9), in comparison with that of the EC(Pt/SnO_2) sensor ($\Delta E_{CO}/\Delta E_{H_2}$: ca. 10). These results indicate that the surface of Pt metal nanoparticles and/or the Pt/SnO_2 interfaces, which were produced by heat treatment in H_2 at 250°C for 1 h, worked as

electrochemically active sites for CO and H_2 oxidation and the electrochemical oxidation activities at these reaction sites of the Pt/SnO_2-h sensing electrode against CO and H_2 were much larger than those at the PtOx-based reaction sites of the Pt/SnO_2 sensing electrode. For the EC(Pd/SnO_2-h) sensor, the electromotive force was quite stable in comparison of that of the EC(Pd/SnO_2) sensor, but both the CO and H_2 responses were much smaller than those of the EC(Pd/SnO_2) sensor. In addition, three kinds of the EC(N/SnO_2-h) sensors (N: Ag, Ir, and Rh) hardly showed CO and H_2 responses, as is the case with the EC(N/SnO_2) sensors (N: Ag, Ir, and Rh). The electrochemical O_2 reduction activity may be too much larger than the electrochemical CO and H_2 oxidation activities at the reaction sites of these N/SnO_2 electrodes and thus these electrode potentials were not able to shift to the negative direction. Except for the EC(N/SnO_2-h) sensors (Au and Pt), only the EC(Ru/SnO_2-h) sensor showed relatively large CO and H_2 responses (ΔE_{CO}: ca. 40 mV, ΔE_{H_2}: ca. 19 mV), but the CO-sensing properties (CO selectivity against H_2 ($\Delta E_{CO}/\Delta E_{H_2}$: ca. 2.1) as well as the magnitude of the CO response) of the EC(Ru/SnO_2-h) sensor were far inferior to those of the EC(Au/SnO_2-h) sensor. Hereafter, we will clarify the effects of the N loading onto the MO surface (MO: SnO_2, especially) on the sensing properties of the EC(N/MO) and EC(N/MO-h) sensors to CO and H_2, to design highly CO sensitive and selective electrochemical gas sensors using an ACP electrolyte and oxide-based electrodes.

4. Conclusions

CO-sensing properties of EC(MO) and EC(N/MO) sensors were measured in wet synthetic air (57%RH) at 30ºC, and effects of the kinds of MO as a base electrode material and N loaded on the MO surface on their CO-sensing properties were investigated in this study. The EC(CeO_2) and EC(Bi_2O_3) sensors showed relatively large CO response and only the EC(Bi_2O_3) sensor responded to H_2, among all the EC(MO) sensors. However, the loading of Au or Pt onto

CeO_2 and Bi_2O_3 was not effective in improving these sensing properties. On the other hand, the EC(In_2O_3) and EC(SnO_2) sensors hardly showed both CO and H_2 responses. However, the Au loading was quite effective in improving the magnitude of CO and H_2 responses of both the EC(In_2O_3) and EC(SnO_2) sensors ($\Delta E_{CO} > \Delta E_{H_2}$). This result indicates that the oxidation of CO and hydrogen adsorbates and the reduction of oxygen adsorbates electrochemically proceeded at the Au/MO interfaces and the number of CO adsorbates was larger than that of hydrogen adsorbates. On the other hand, the Pt loading largely enhanced the magnitude of CO response of the EC(SnO_2) sensor, but was not so much effective in improving the magnitude of H_2 response. Therefore, the EC(Pt/SnO_2) sensor showed the most excellent CO selectivity against H_2, among all the sensors in this study. The XPS spectra of the Pt/SnO_2 and the sensing properties of the EC(Pt/SnO_2) sensor suggest that the large number of CO molecules was easily adsorbed on Pt^{4+} sites and/or via oxygen vacancies next to Pt^{4+} at the surface lattice of SnO_2. Among other EC(N/SnO_2) sensors, only the EC(Pd/SnO_2) sensor showed large CO and H_2 responses, together with the operating instability which was caused by the oxidation of Pd-based reaction sites. The heat treatment of N/MO powders in H_2 250°C had various impacts on their CO and H_2 responses in some cases. Namely, the heat treatment largely reduced the CO and H_2 responses of the EC(Pd/SnO_2) sensor, moderately increased the CO and H_2 responses of the EC(Ru/SnO_2) sensor, improved the CO selectivity of the EC(Au/SnO_2) sensor against H_2 together with a considerable decrease in the H_2 response, and enhanced both CO and H_2 responses of the EC(Pt/SnO_2) sensor, leading to a decrease in its CO selectivity against H_2.

References

[1] WHO Regional Office for Europe, Copenhagen, Denmark, Air quality guidelines for Europe, 2nd edition (CD ROM version), WHO Regional Publications, European Series, No. 91 (2000).

[2] D. Koziej, N. Bârsan, K. Shimanoe, N. Yamazoe, J. Szuber, U. Weimar, Spectroscopic insights into CO sensing of undoped and palladium doped tin dioxide sensors derived from hydrothermally treated tin oxide sol, Sens. Actuators B 118 (2006) 98–104.

[3] J. W. Fergus, Solid electrolyte based sensors for the measurement of CO and hydrocarbon gases, Sen. Actuators B 122 (2007) 683–693.

[4] N. Izu, I. Matsubara, T. Itoh, W. Shin, Performance of a carbon monoxide sensor based on zirconia-doped ceria, J. Asian Ceram. Soc. 4 (2016) 205–208.

[5] Y. Shimizu, S. Yamamoto, S. Takase, A thick-film impedancemetric carbon monoxide sensor using layered perovskite-type cuprate, Sens. Actuators B 249 (2017) 667–672.

[6] T. Goto, T. Itoh, T. Akamatsu, T. Sekino, W. Shin, Relationship between the CO sensing performance of micro-thermoelectric gas sensors and characteristics of PtPd/Co_3O_4 and PtPd/SnO_2 catalysts, Sens. Actuators B 243 (2017) 847–855.

[7] N. Miura, H. Kato, H. Yamazoe, T. Seiyama, A proton conductor gas sensor operative at ordinary temperature, Denki Kagaku (presently Electrochemistry) 50 (1982) 858–859.

[8] N. Miura, H. Kato, N. Yamazoe, and T. Seiyama, An improved type of proton conductor sensor sensitive to H_2 and CO at room temperature, Chem. Lett. 12 (1983) 1573–1576.

[9] P. D. van del Wal, N. F. de Rooij, M. Koudelka-Hep, Extremely stable Nafion based carbon monoxide sensor, Sens. Actuators B 35 (1996) 119–123.

[10] R. J. Mortimer, A. Beech, AC impedance characteristics of solid-state planar electrochemical carbon monoxide sensors with Nafion® as solid polymer electrolyte, Electrochim. Acta 47 (2002) 3383–3387.

[11] K. Mochizuki, T. Kikuchi, M. Sudoh, Y. Ishiguro, T. Suzuki, Performances of fuel-cell-type CO sensors using each of polybenzimidazole and Nafion membranes, J. Electrochem. Soc. 158 (2011) J71–J75.

[12] Y. Guan, M. Dai, T. Liu, Y. Liu, F. Liu, X. Liang, H. Suo, P. Sun, G. Lu, Effect of the dispersants on the performance of fuel cell type CO sensor with Pt–C/Nafion electrodes, Sens. Actuators B 230 (2016) 61–69.

[13] Y. Guan, F. Liu, B. Wang, X. Yang, X. Liang, H. Suo, P. Sun, Y. Sun, J. Ma, J. Zheng, Y. Wang, G. Lu, Highly sensitive amperometric Nafion-based CO sensor using Pt/C electrodes with different kinds of carbon materials, Sens. Actuators B 239 (2017) 696–703.

[14] K. Izawa, Introduction of carbon monoxide gas sensors and their application, Chemical Sensors 34 (2018) 8–13.

[15] H. Yanagi, K. Fukuda, Anion exchange membrane and ionomer for alkaline membrane fuel cells (AMFCs), ECS Trans. 16(2) (2008) 257–262.

[16] K. Fukuta, H. Inoue, S. Watanabe, H. Yanagi, In-situ observation of CO2 through the self-purging in alkaline membrane fuel cell (AMFC), ECS Trans. 19(31) (2009) 23–27.

[17] K. Matsumoto, T. Fujigaya, H. Yanagi, N. Nakashima, Very high performance alkali anion-exchange membrane fuel cells, Adv. Funct. Mater. 21 (2011) 1089–1094.

[18] T. Hyodo, C. Ishibashi, H. Yanagi, K. Kaneyasu, Y. Shimizu, Potentiometric hydrogen sensors using an anion-conducting polymer as an electrolyte, Reports of the Faculty of Engineering, Nagasaki University 42(79) (2012) 42–47.

[19] T. Goto, T. Hyodo, K. Kaneyasu, H. Yanagi, and Y. Shimizu, CO sensing properties of electrochemical gas sensors using an anion-conducting polymer as an electrolyte, ECS Trans. 50(12) (2013) 267–272.

[20] T. Hyodo, C. Ishibashi, K. Matsuo, K. Kaneyasu, H. Yanagi, Y. Shimizu, CO and CO_2

sensing properties of electrochemical gas sensors using an anion-conducting polymer as an electrolyte, Electrochim. Acta 82 (2012) 19–25.

[21] T. Goto, T. Hyodo, T. Ueda, K. Kamada, K. Kaneyasu, Y. Shimizu, CO-sensing properties of potentiometric gas sensors using an anion-conducting polymer electrolyte and Au-loaded metal oxide electrodes, Electrochim. Acta 166 (2015) 232–243.

[22] T. Hyodo, T. Goto, T. Ueda, K. Kaneyasu, Y. Shimizu, Potentiometric carbon monoxide sensors using an anion-conducting polymer electrolyte and Au-loaded SnO_2 electrodes, J. Electrochem. Soc. 163 (2016) B300–B308.

[23] L.-F. Gutierrez, S. Hamoudi, K. Belkacemi, Synthesis of gold catalysts supported on mesoporous silica materials: recent developments Catalysts 1 (2011) 97–154.

[24] K. S. W. Sing, Reporting physisorption data for gas/solid systems with special reference to the determination of surface area and porosity, Pure Appl. Chem. 54 (1982) 2201–2218.

[25] Kurt J. Lesker Co., Installation and operation manual of FTC-2800 (thin film deposition controller), Ver. 6.10 (2009).

[26] T. Ueda, H. Takeda, K. Kamada, T. Hyodo, Y. Shimizu, Enhanced CO response of NASICON-based gas sensors using oxide-added Pt sensing electrode at low temperature operation, Electrochemistry 85 (2017) 174–178.

[27] M. Hübner, D. Koziej, M. Bauer, N. Barsan, K. Kvashnina, M. D. Rossell, U. Weimar, J.-D. Grunwaldt, The structure and behavior of platinum in SnO_2-based sensors under working conditions, Angew. Chem. Int. Ed. 50 (2011) 2841–2844.

[28] N. Murata, T. Suzuki, M. Kobayashi, F. Togoh, K. Asakura, Characterization of Pt-doped SnO_2 catalyst for a high-performance micro gas sensor, Phys. Chem. Chem. Phys. 15 (2013) 17938–17946.

[29] R. D. Shannon, Revised effective ionic radii and systematic studies of interatomic distances in halides and chalcogenides, Acta Cryst. A32 (1976) 751–767.

[30] M. Daté, Y. Ichihashi, T. Yamashita, A. Chiorino, F. Boccuzzi, M. Haruta, Performance of Au/TiO_2 catalyst under ambient conditions, Catal. Today 72 (2002) 89–94.

[31] T. Fujitani, I. Nakamura, Mechanism and active sites of the oxidation of CO over Au/TiO_2, Angew. Chem. Int. Ed. 50 (2011) 10144–10147.

[32] M. Haruta, Chance and necessity: My encounter with gold catalysts, Angew. Chem. Int. Ed. 53 (2014) 52–56.

[33] B. Hammer, J. K. Norskov, Why gold is the noblest of all the metals, Nature 376 (1995) 238–241.

[34] T. Fujitani, I. Nakamura, T. Akita, M. Okumura, M. Haruta, Hydrogen dissociation by gold clusters, Angew. Chem. Int. Ed. 48 (2009) 9515–9518.

[35] P. Torruella, C. Coll, G. Martín, L. López-Conesa, M. Vila, C. Díaz-Guerra, M. Varela, M. L. Ruiz-González, J. Piqueras, F. Peiró, S. Estradé, Assessing oxygen vacancies in bismuth oxide through EELS measurements and DFT simulations, J. Phys. Chem. C 121 (2017) 24809–24815.

[36] T. Sakamoto, M. Egashira, T. Seiyama, New catalytic aromatization of lower olefins over bismuth phosphate catalyst, J. Catal. 16 (1970) 407–409.

[37] Y. Lou, L. Wang, Z. Zhao, Y. Zhang, Z. Zhang, G. Lu, Y. Guo, Y. L. Guo, Low-temperature CO oxidation over Co_3O_4-based catalysts: Significant promoting effect of Bi_2O_3 on Co_3O_4 catalyst, Appl. Catal. B 146 (2014) 43–49.

[38] Y.-G. Cho, B.-H. Hwang, D.-W. Park, H.-C. Woo, J.-S. Chung, Phase cooperation of V_2O_5 and Bi_2O_3 in the selective oxidation of H_2S containing ammonia and water, Korean J. Chem. Eng. 19 (2002) 611–616.

[39] H. Takeda, T. Ueda, K. Kamada, K. Matsuo, T. Hyodo, Y. Shimizu, CO-sensing properties of a NASICON-based gas sensor attached with Pt mixed with Bi_2O_3 as a sensing electrode, Electrochem. Acta 155 (2015) 8–15.

[40] E. N. Voskresenskaya, L. I. Kurteeva, A. G. Anshits, Solid solutions of bismuth oxide as promising catalysts for oxidative coupling of methane, Appl. Catal. A 90 (1992) 209–216.

[41] C. Song, J. Zhang, Electrocatalytic oxygen reduction reaction, in: J. Zhang (Ed.), PEM Fuel Cell Electrocatalysts and Catalyst Layers, Springer, Berlin, 2008, pp. 89–134.

Figure Captions

Fig. 1. Schematic drawings of (a) sensor element and (b) gas-sensing measurement system with two electrode compartments.

Fig. 2. Response transients of EC(MO) and EC(N/MO) sensors (MO: Bi_2O_3, CeO_2, In_2O_3, SnO_2, and V_2O_5, N: Au and Pt) to 500 ppm CO in wet synthetic air at 30ºC (57%RH).

Fig. 3. Response transients of EC(MO) and EC(N/MO) sensors (MO: Bi_2O_3, CeO_2, In_2O_3, SnO_2, and V_2O_5, N: Au and Pt) to 500 ppm H_2 in wet synthetic air at 30ºC (57%RH).

Fig. 4. XPS spectra of Au 4f and Pt 4f of N/MO powders (N: Au and Pt, MO: Bi_2O_3, In_2O_3, and SnO_2).

Fig. 5. XPS spectra of Bi $4f_{7/2}$ of N/Bi_2O_3 powder, In $4f_{7/2}$ of N/In_2O_3 powder, and Sn $3d_{5/2}$ of N/SnO_2 powder (N: Au and Pt).

Fig. 6. XPS spectra of O 1s of N/MO powders (N: Au and Pt, MO: Bi_2O_3, In_2O_3, and SnO_2).

Fig. 7. Response transients of EC(Au) and EC(Pt) sensors to 500 ppm CO and 500 ppm H_2 in wet synthetic air at 30ºC (57%RH).

Fig. 8. Response transients of EC(N/SnO_2) sensors (N: Ag, Au, Ir, Rh, Ru, Pd, and Pt) to (a) 500 ppm CO and (b) 500 ppm H_2 in wet synthetic air at 30ºC (57%RH).

Fig. 9. XRD spectra of Pd 3d of Pd/SnO_2 sensing electrode of EC(Pd/SnO_2) sensor before and after exposure to 3000 ppm CO and H_2 balanced with wet synthetic air for 2 h.

Fig. 10. Response transients of EC(N/SnO_2-h) sensors (N: Ag, Au, Ir, Rh, Ru, Pd, and Pt) to (a) 500 ppm CO and (b) 500 ppm H_2 in wet synthetic air at 30ºC (57%RH).

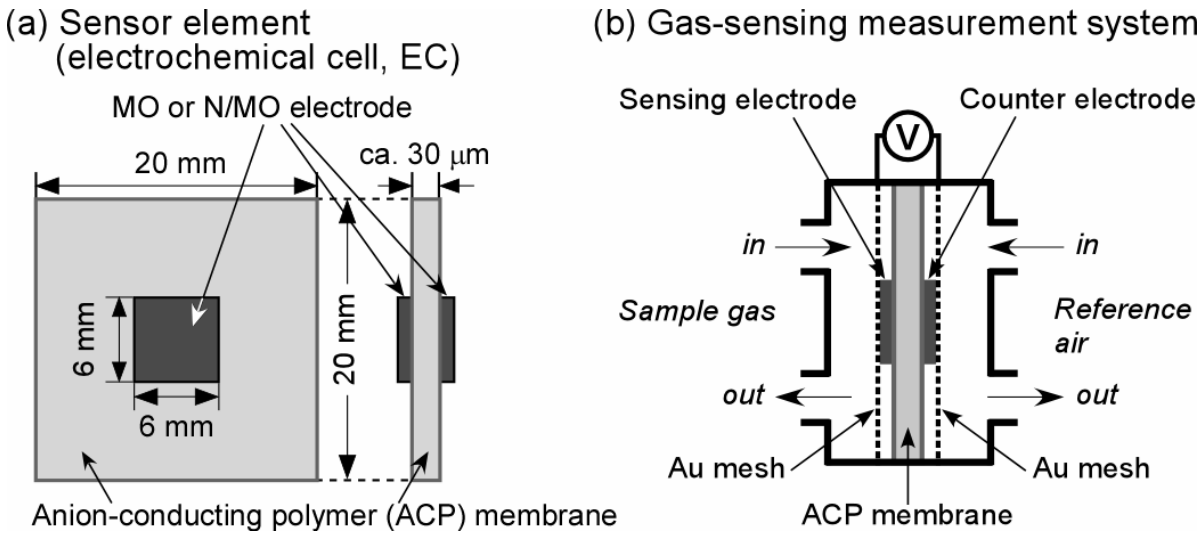

Fig. 1. Hyodo et al.

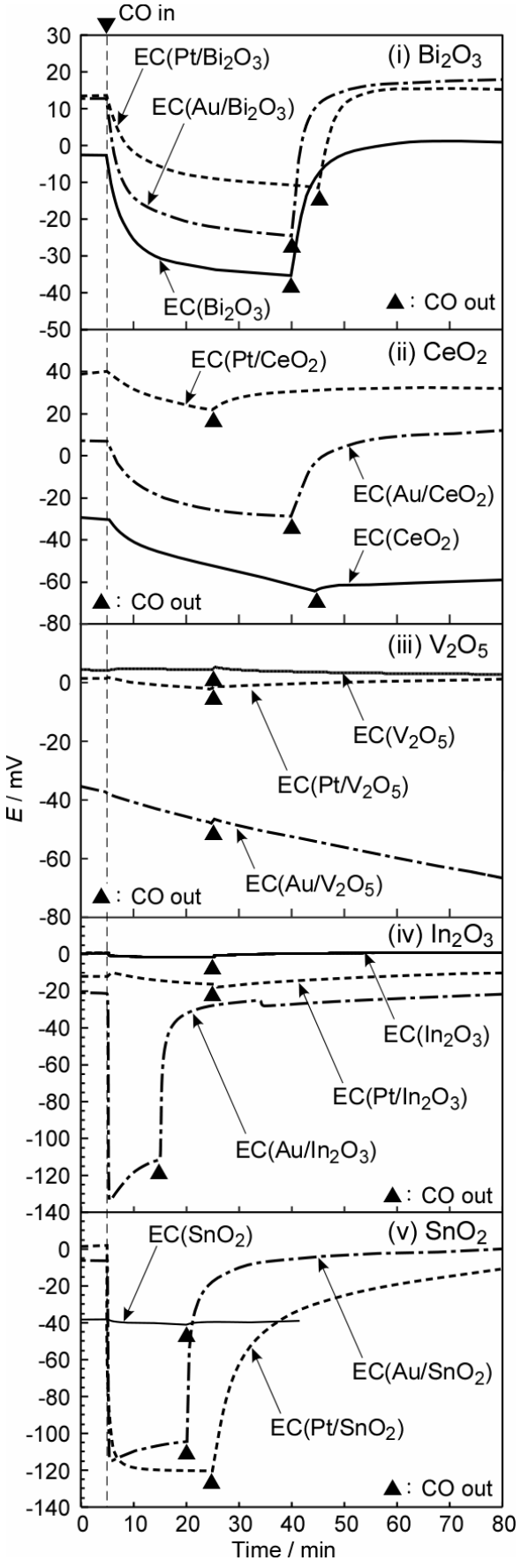

Fig. 2. Hyodo et al.

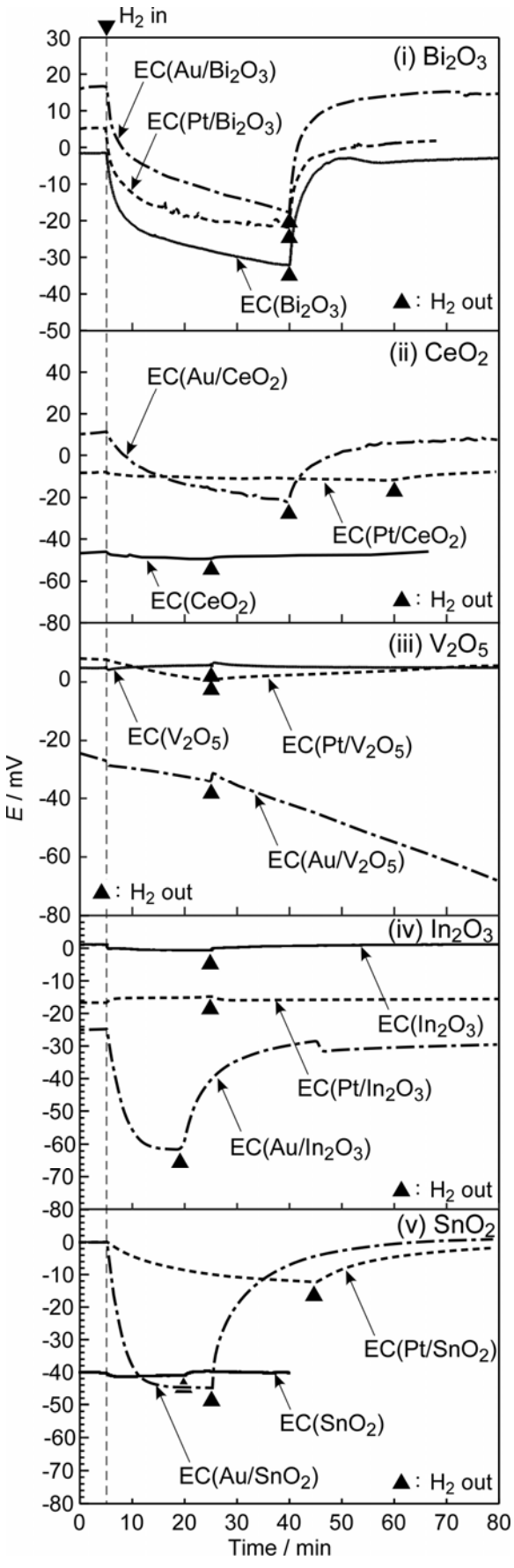

Fig. 3. Hyodo et al.

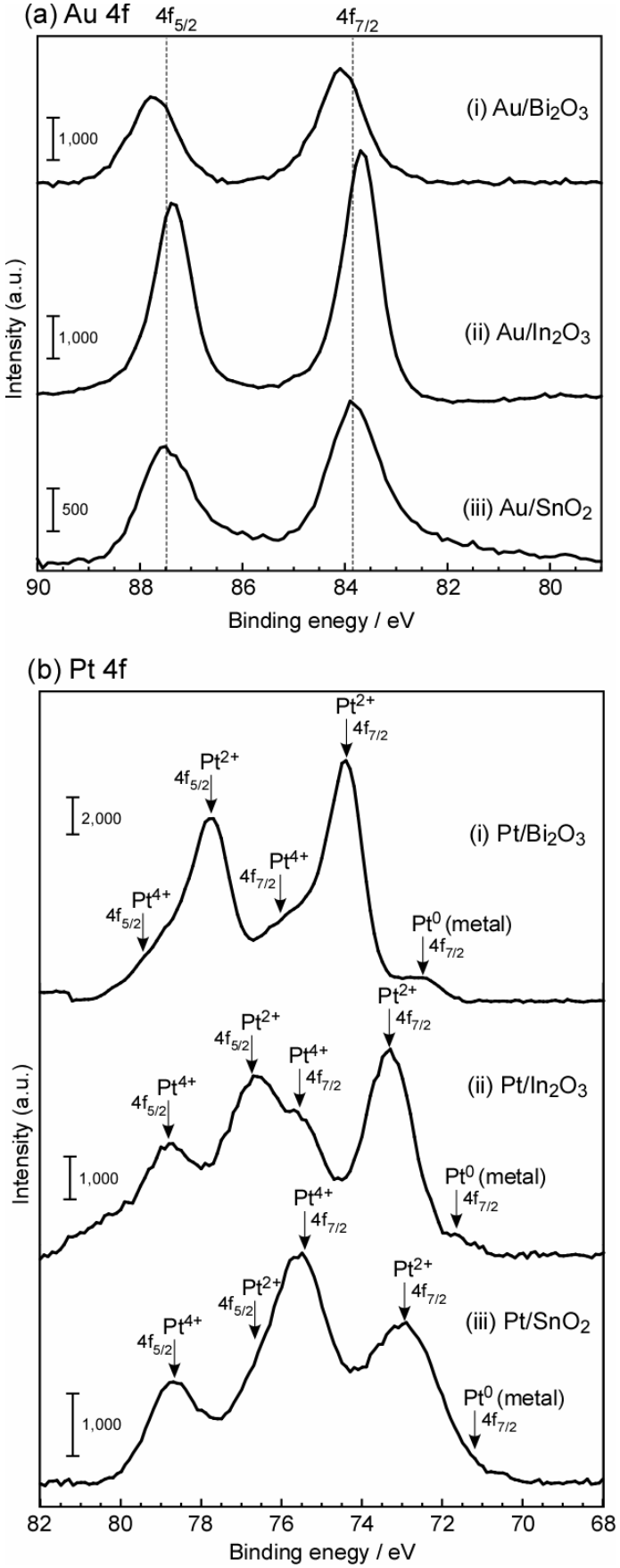

Fig. 4. Hyodo et al.

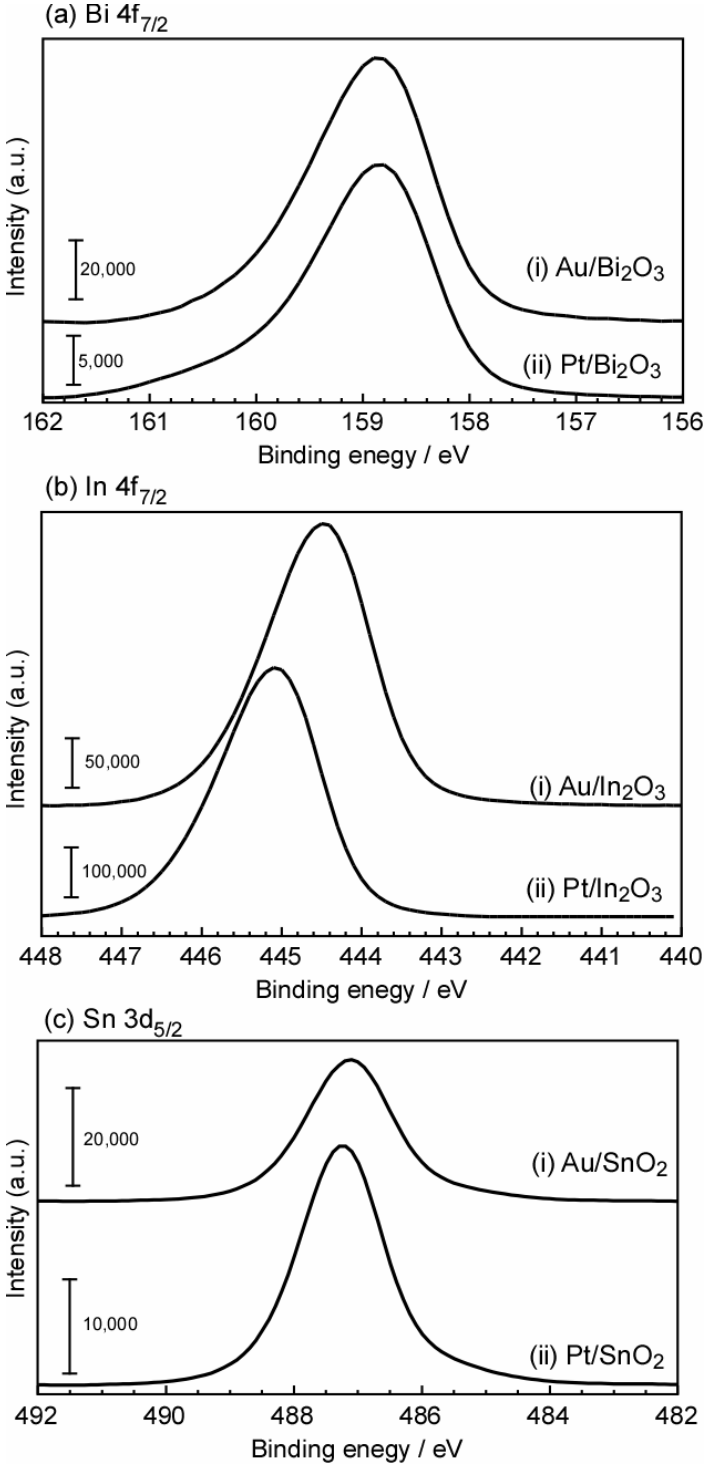

Fig. 5. Hyodo et al.

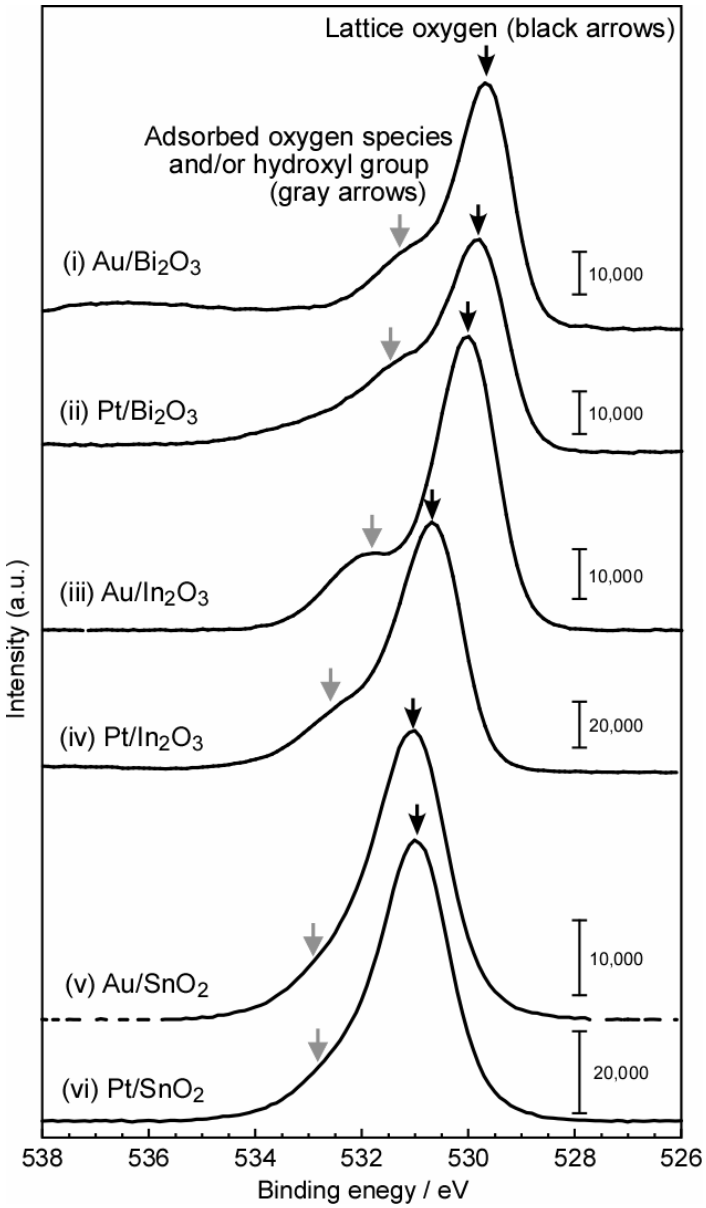

Fig. 6. Hyodo et al.

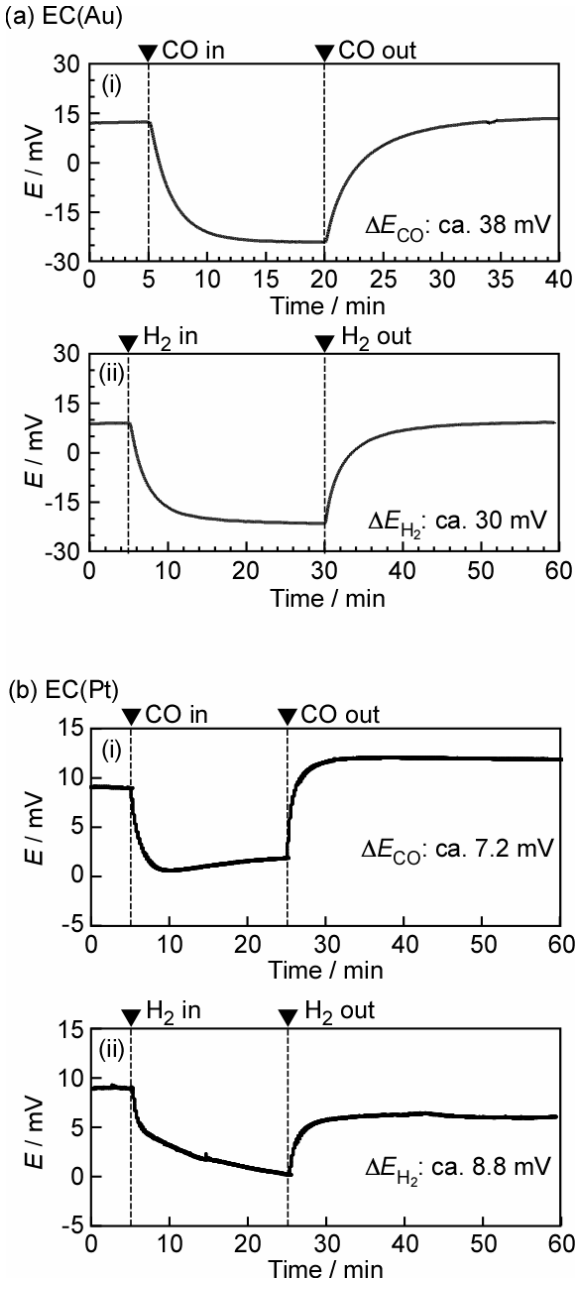

Fig. 7. Hyodo et al.

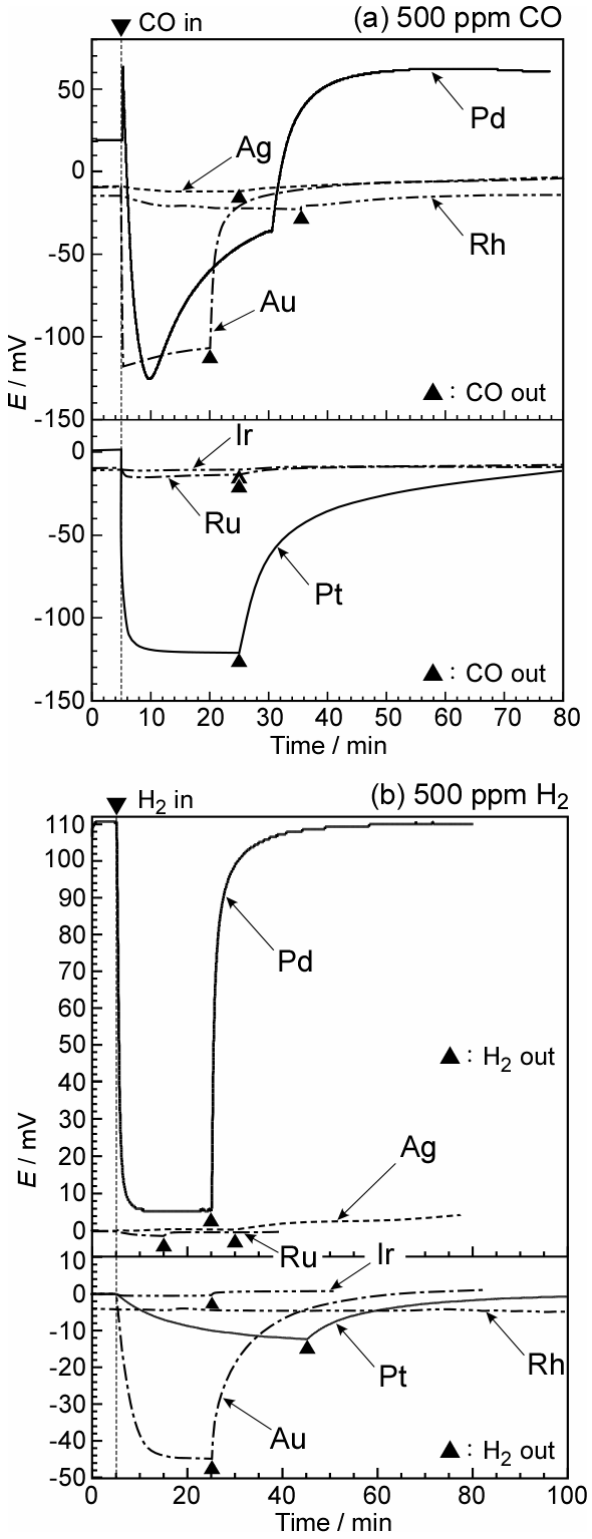

Fig. 8. Hyodo et al.

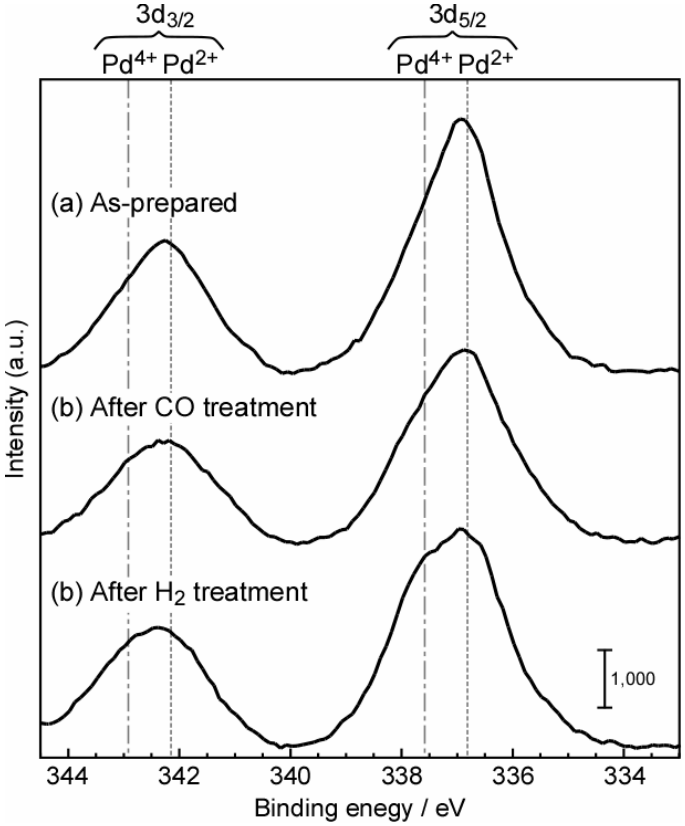

Fig. 9. Hyodo et al.

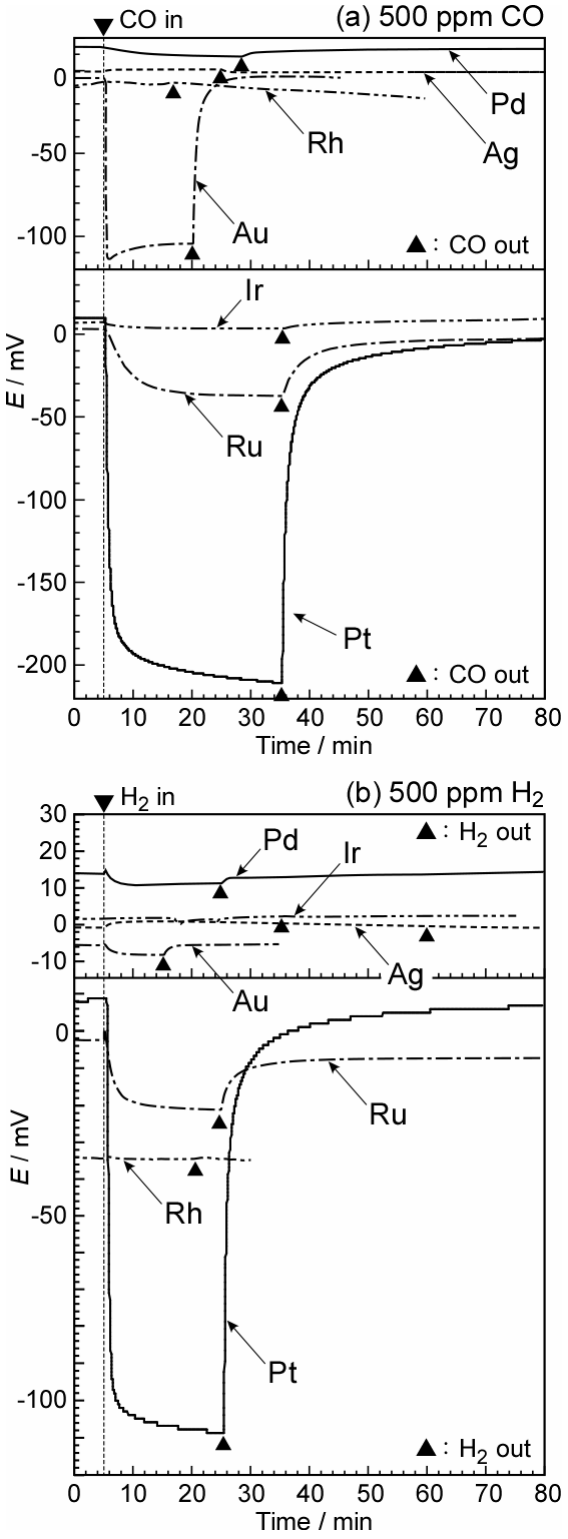

Fig. 10. Hyodo et al.

Supporting Information

Potentiometric CO sensors using anion-conducting polymer electrolyte: effects of the kinds of noble metal-loaded metal oxides as sensing-electrode materials on CO-sensing properties

Takeo Hyodo*, Mari Takamori, Toshiyuki Goto, Taro Ueda, and Yasuhiro Shimizu

Graduate School of Engineering, Nagasaki University
1-14 Bunkyo-machi, Nagasaki 852-8521, Japan

*Corresponding author: hyodo@nagasaki-u.ac.jp

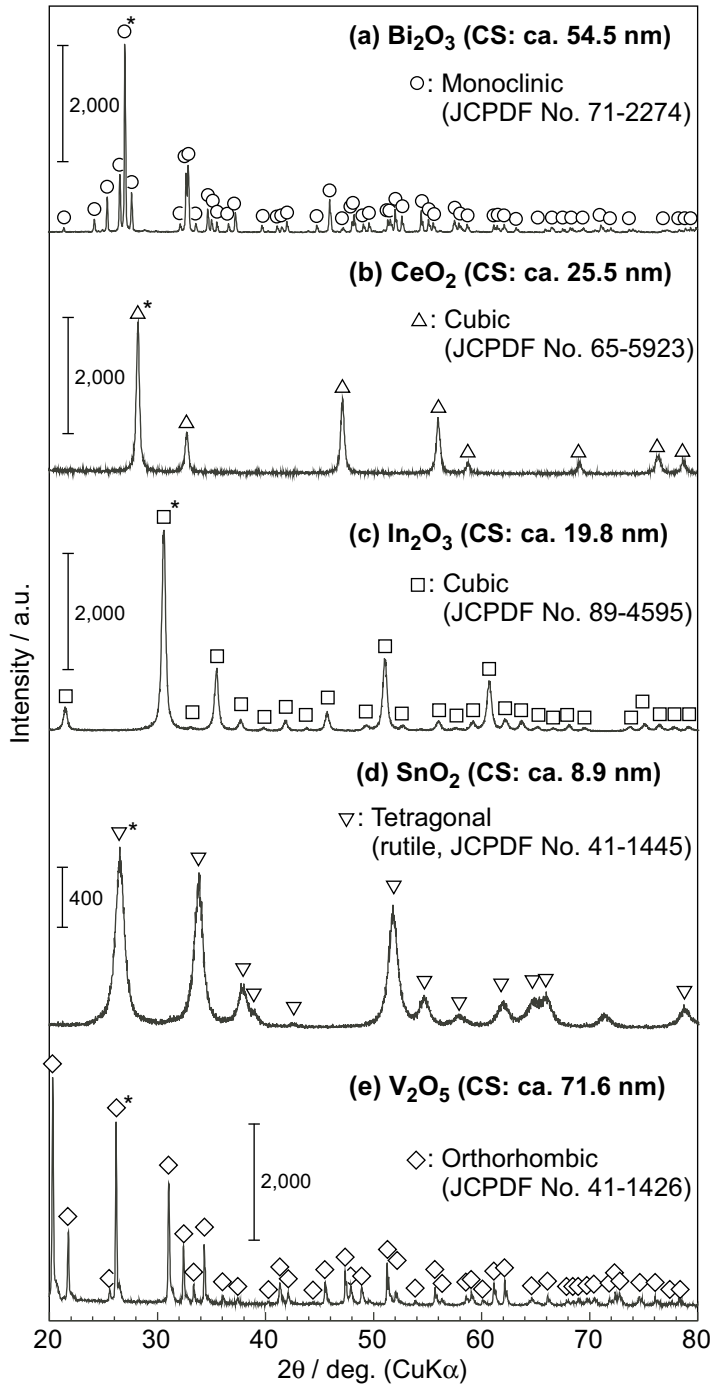

Figure S1. XRD spectra of all metal-oxide (MO) powders, together with crystallite sizes (CSs).
*: Diffraction peaks utilized for calculation of CSs.

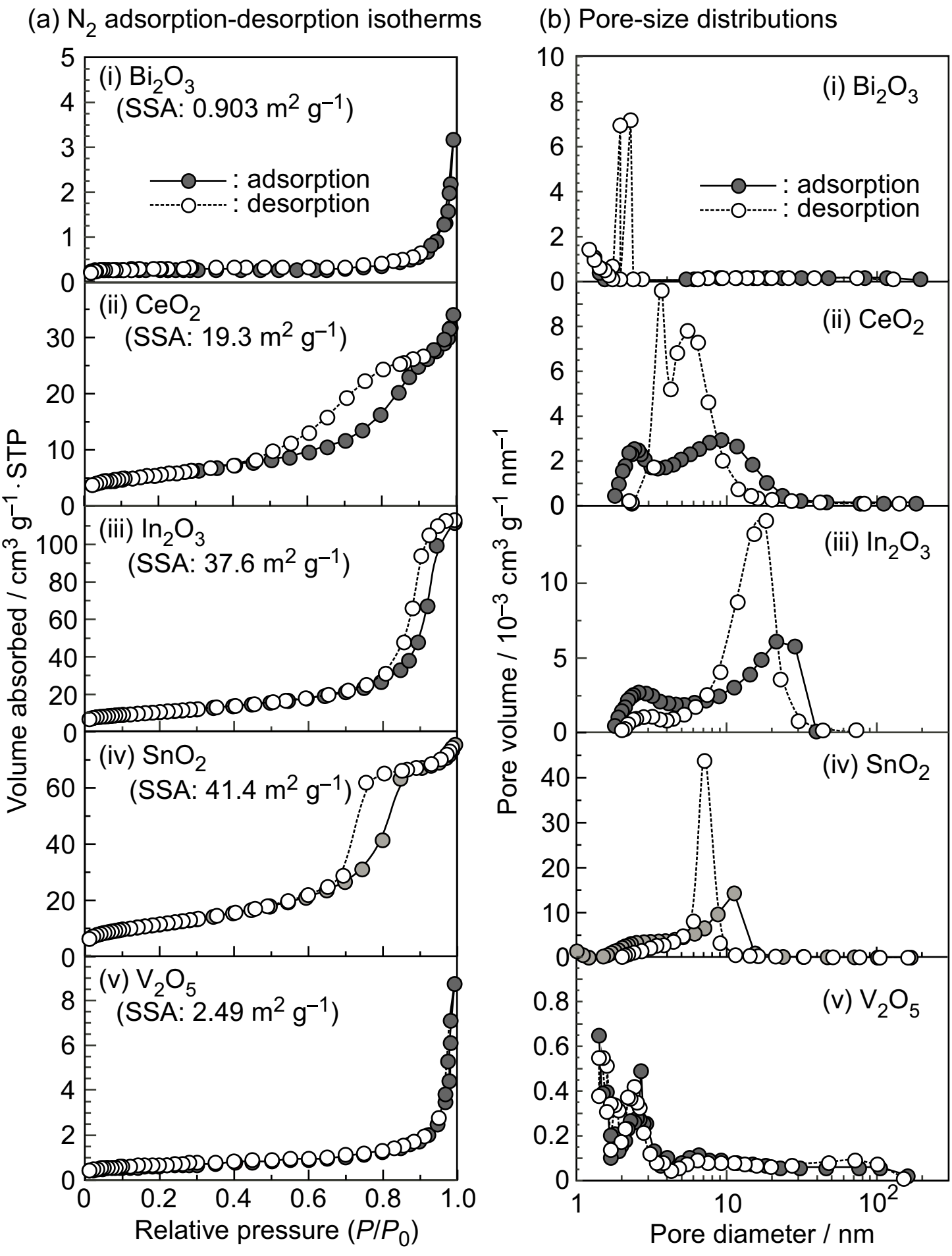

Figure S2. N_2 adsorption-desorption isotherms with specific surface areas (SSAs) and pore-size distributions of all MO powders.

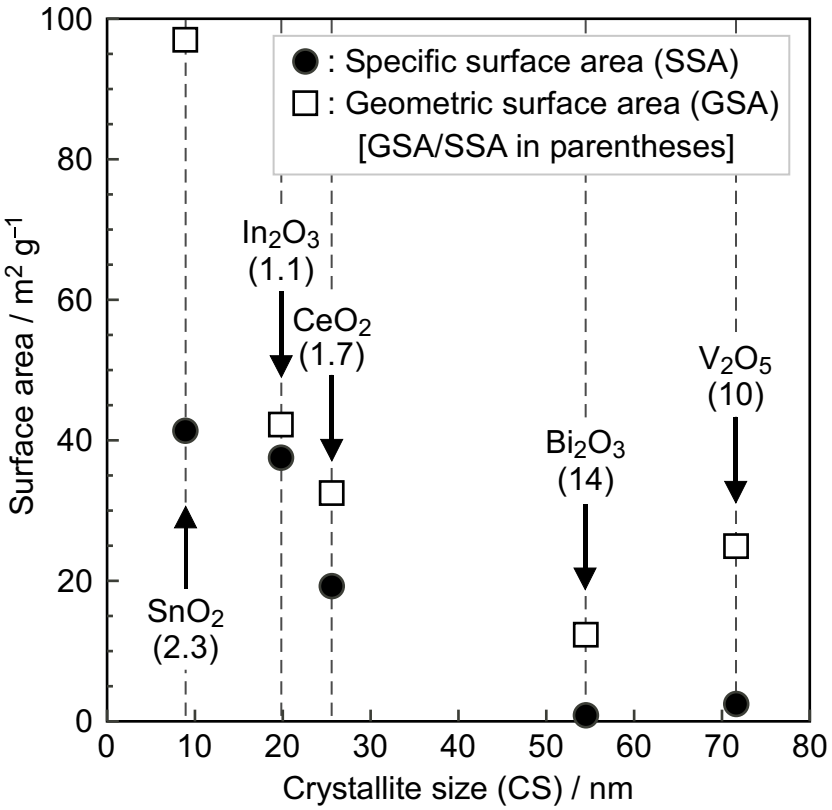

Figure S3. Relationship between two kinds of surface areas (SSA and GSA) and CS of all MO powders.

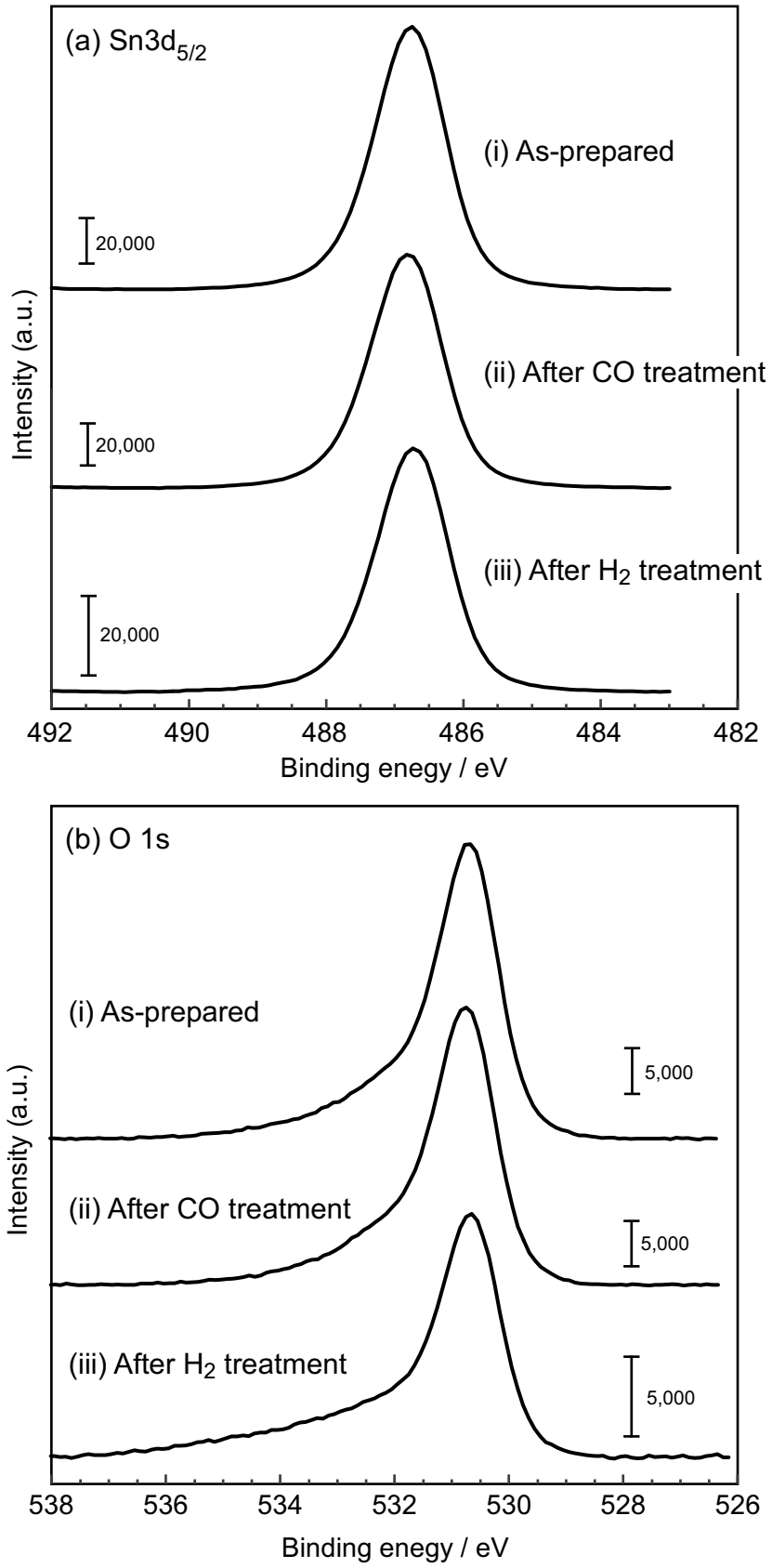

Figure S4. XPS spectra of Sn $3d_{5/2}$ and O 1s of Pd/SnO_2 sensing electrode of EC(Pd/SnO_2) sensor before and after exposure to 3000 ppm CO and H_2 balanced with wet synthetic air for 2 h.